The Astrophysical Journal, 996:143 (14pp), 2026 January 10 https://doi.org/10.3847/1538-4357/ae1838

The Jetted Tidal Disruption Event AT 2022cmc: Investigating Connections to the Optical Tidal Disruption Event Population and Spectral Subclasses through Late-time Follow-up

Erica Hammerstein[1], S. Bradley Cenko[2], Igor Andreoni[3], Panos Charalampopoulos[4], Ryan Chornock[1], Raffaella Margutti[1,5], Brendan O'Connor[6], Steve Schulze[7], Jesper Sollerman[8], Sudhanshu Barway[9], Varun Bhalerao[10], G. C. Anupama[9], Harsh Kumar[11], Ester Marini[12], Diego Paris[12], Daniel A. Perley[13], Andrea Rossi[14], and Yuhan Yao[1,15]

[1] Department of Astronomy, University of California, Berkeley, CA 94720, USA; ekhammer@berkeley.edu
[2] Astrophysics Science Division, NASA Goddard Space Flight Center, Mail Code 661, Greenbelt, MD 20771, USA
[3] University of North Carolina at Chapel Hill, 120 East Cameron Avenue, Chapel Hill, NC 27514, USA
[4] Department of Physics and Astronomy, FI-20014, University of Turku, Finland
[5] Department of Physics, University of California, 366 Physics North MC 7300, Berkeley, CA 94720, USA
[6] McWilliams Center for Cosmology and Astrophysics, Department of Physics, Carnegie Mellon University, Pittsburgh, PA 15213, USA
[7] Center for Interdisciplinary Exploration and Research in Astrophysics (CIERA), Northwestern University, 1800 Sherman Avenue, Evanston, IL 60201, USA
[8] Department of Astronomy, The Oskar Klein Center, Stockholm University, AlbaNova University Center, SE 106 91 Stockholm, Sweden
[9] Indian Institute of Astrophysics, II Block Koramangala, Bengaluru 560034, India
[10] Department of Physics, Indian Institute of Technology Bombay, Powai 400076, India
[11] Center for Astrophysics | Harvard & Smithsonian, 60 Garden Street, Cambridge, MA 02138-1516, USA
[12] INAF - Osservatorio Astronomico di Roma, Via Frascati 33, 00078 Monteporzio Catone, Rome, Italy
[13] Astrophysics Research Institute, Liverpool John Moores University, IC2, Liverpool Science Park, 146 Brownlow Hill, Liverpool L3 5RF, UK
[14] INAF - Osservatorio di Astrofisica e Scienza dello Spazio di Bologna, via Piero Gobetti 93/3, I-40129 Bologna, Italy
[15] Miller Institute for Basic Research in Science, 468 Donner Lab, Berkeley, CA 94720, USA
Received 2025 June 9; revised 2025 October 7; accepted 2025 October 22; published 2026 January 9

Abstract

AT 2022cmc is the first on-axis jetted tidal disruption event (TDE) to be discovered at optical wavelengths. The optically bright nature of AT 2022cmc presents an unprecedented opportunity to place this jetted TDE in the context of the larger optically selected thermal TDE population and explore potential connections to optical TDE subclasses, particularly the class of luminous TDEs that lack optical spectral features. In this work, we present late-time optical observations of AT 2022cmc, both imaging and spectroscopy, that extend the optical dataset to ∼160 days from the first detection in the observed frame. The light curve clearly evolves from red to blue, which we interpret as a transition from a nonthermally dominated spectral energy distribution (SED) to thermally dominated SED. By accounting for the nonthermal emission evident in the optical SED at early times, we extract the properties of the thermal emission and compare to a sample of optically selected thermal TDEs. We find that the properties of AT 2022cmc are consistent with previous correlations found for the evolution and properties of thermal TDEs, with the thermal properties of AT 2022cmc aligning with the class of featureless and luminous TDEs. The confirmation of this similarity motivates the importance of prompt and multiwavelength follow-up of featureless and luminous TDEs in order to further explore the connection they have with jetted TDEs.

Unified Astronomy Thesaurus concepts: Transient sources (1851); Tidal disruption (1696); Black holes (162); Relativistic jets (1390)

Materials only available in the online version of record: machine-readable table

1. Introduction

Every so often (∼10^4 yr) in the nucleus of a galaxy, a star will wander too close to the supermassive black hole (SMBH) lurking there and will be subsequently torn apart by the tidal forces and accreted by the SMBH (J. G. Hills 1975; J. Frank & M. J. Rees 1976). These tidal disruption events (TDEs) create luminous flares of radiation visible from Earth. Samples of TDEs have now been discovered across the electromagnetic spectrum from X-ray (e.g., S. Komossa & N. Bade 1999; S. Sazonov et al. 2021) to optical (e.g., S. Gezari et al. 2012; E. Hammerstein et al. 2023a; Y. Yao et al. 2023), infrared (e.g., M. Masterson et al. 2024), and radio (e.g., J. J. Somalwar et al. 2025).

The advent of all-sky optical surveys, such as PanSTARRS (K. C. Chambers et al. 2016), ASAS-SN (B. J. Shappee et al. 2014), and the Zwicky Transient Facility (ZTF; E. C. Bellm et al. 2019; M. J. Graham et al. 2019), in the last ∼20 yr has led to the majority of current TDE discoveries being made at these wavelengths. These optically selected TDEs are typically dominated by a hot (10^4–10^5 K), thermal continuum with rise timescales of ∼30 days, peak absolute magnitudes of $M_r \sim -17$ to -22 mag (e.g., see Figure 9 of Y. Yao et al. 2023), and fade timescales of 200–400 days (e.g., S. van Velzen et al. 2021; E. Hammerstein et al. 2023a). Optically selected TDEs show a broad range of emissions at other wavelengths, including a variety of behaviors in the X-ray, such as late-time brightening, flaring, and power-law decaying (e.g., S. van Velzen et al. 2021; M. Guolo et al. 2024; E. Hammerstein et al. 2023a; Y. Yao et al. 2024b). The optical spectra of TDEs are most often characterized by broad emission features (e.g., P. Charalampopoulos et al. 2022;

E. Hammerstein et al. 2023a), with S. van Velzen et al. (2021) formalizing a classification scheme based on the observed lines being primarily Balmer or He II, known as TDE-H or TDE-He, respectively, or a combination with occasional evidence for Bowen fluorescence emission, known as TDE-H+He. E. Hammerstein et al. (2023a) put forth an additional spectroscopic class of TDEs called TDE-featureless that show no discernible emission lines or spectroscopic features present in the three other classes, although host galaxy absorption lines can be observed. This featureless class of TDEs is characterized by higher peak luminosities ($M_r \sim -21$ mag), peak blackbody temperatures ($T_{\rm BB} \gtrsim 10^{4.4}$ K), and peak blackbody radii ($R_{\rm BB} \gtrsim 10^{15.4}$ cm). Their host galaxies are often more massive, potentially implying more massive black holes, and redder than typical TDE hosts, which tend to favor "green" galaxies (e.g., J. Law-Smith et al. 2017; E. Hammerstein et al. 2021).

TDEs discovered at other wavelengths, such as in the soft X-ray, are also characterized by thermal emission, though the thermal continuum in X-ray selected events is typically much hotter than their optically selected counterparts (see S. Gezari 2021, for a review). A very small fraction of TDEs have been discovered through nonthermal emission from an on-axis, collimated, relativistic jet (hereafter "jetted TDE"). Three of these objects were discovered more than a decade ago by the hard X-ray Burst Alert Telescope (BAT; S. D. Barthelmy et al. 2005) aboard the Neil Gehrels Swift Observatory (N. Gehrels et al. 2004). These candidates include Sw J1644+57 (J. S. Bloom et al. 2011; D. N. Burrows et al. 2011; A. J. Levan et al. 2011; B. A. Zauderer et al. 2011), Sw J2058+05 (S. B. Cenko et al. 2012; D. R. Pasham et al. 2015), and Sw J1112-82 (G. C. Brown et al. 2015, 2017). Some of these jetted TDEs have shown faint or late-time optical counterparts. Jetted TDEs provide an important opportunity to study the launching of relativistic jets by SMBHs, the jet emission mechanism, and the jet composition (for a review, see F. De Colle & W. Lu 2020).

Recently, a fourth candidate jetted TDE was reported. In contrast to the previous three candidates, AT 2022cmc (ZTF22aaajecp) was discovered by ZTF as an optical transient (I. Andreoni et al. 2022). The first detection in the optical on 2022 February 11 was shortly followed by detections in the radio (D. A. Perley 2022), submillimeter (D. A. Perley et al. 2022), and X-ray (D. Pasham et al. 2022). The emission across wavelengths is exceptionally luminous, and the redshift ($z = 1.193$) provided by follow-up spectroscopy (N. R. Tanvir et al. 2022) implies an absolute optical luminosity of $M_i \approx -25$ mag at peak (I. Andreoni et al. 2022). The follow-up observations revealed remarkable similarities to the jetted TDE Sw J1644+47, including long-lived X-ray emission with short timescale variability and a drop in flux at late times due to jet shut-off (T. Eftekhari et al. 2024), and corresponding radio and infrared counterparts (J. S. Bloom et al. 2011; D. N. Burrows et al. 2011; A. J. Levan et al. 2011). Sw J1644+57 was not detected in the optical or ultraviolet until much later (A. J. Levan et al. 2016), although this is unsurprising due to the large inferred host galaxy extinction (D. N. Burrows et al. 2011). Because of these similarities, and after ruling out other possible transients such as a kilonova, a luminous fast blue optical transient, blazar, or a γ-ray burst, the interpretation of AT 2022cmc as a jetted TDE is favored (I. Andreoni et al. 2022; D. R. Pasham et al. 2023; L. Rhodes et al. 2023).

While AT 2022cmc is the first optically selected jetted TDE, it fits the general picture established by prior X-ray selected events. In the X-ray, all known jetted TDEs have been shown to have a transition from variable X-ray in the first few days which shuts off at later times, interpreted as an accretion state change from super-Eddington to sub-Eddington (G. C. Brown et al. 2015; D. R. Pasham et al. 2015; T. Eftekhari et al. 2024). This is indeed observed for AT 2022cmc (T. Eftekhari et al. 2024). In the radio and millimeter, Sw J1644+47 was observed to have a bright counterpart associated with synchrotron emission from a collimated relativistic jet (B. A. Zauderer et al. 2011; E. Berger et al. 2012), which has also been shown for AT 2022cmc. For events where an optical spectrum was obtained (namely, AT 2022cmc and Sw J2058 +05), they appear to be dominated by a featureless, blue continuum, the origin of which has not yet been explained (D. R. Pasham et al. 2015; I. Andreoni et al. 2022). Until now, jetted TDE studies have focused on the nonthermal emission from a relativistic jet because no (or very faint) optical counterparts consistent with thermal emission have been detected. AT 2022cmc is the first event for which direct comparisons to the general thermal TDE population may be made.

Interestingly, AT 2022cmc's UV, optical, and IR light curve is characterized by a red color which turns bluer after several days postpeak (hereafter "red phase" and "blue phase," respectively). This contrasts with the typical evolution of optical TDEs, which show little evolution from their initial blue colors throughout their light curves (e.g., S. van Velzen et al. 2021; E. Hammerstein et al. 2023a; Y. Yao et al. 2023). I. Andreoni et al. (2022) interpret this fast-fading red flare as synchrotron emission resulting from the jet's interaction with the circumnuclear medium. The slower-evolving, blue, thermal optical/UV emission is thought to have origins similar to nonjetted TDEs, which may come from the reprocessing of X-ray emission originating in the accretion disk to the UV and optical by a wind or outflow (A. Loeb & A. Ulmer 1997; J. Guillochon et al. 2014; L. Dai et al. 2018), or shocks and subsequent outflows created by intersecting stellar debris streams (T. Piran et al. 2015; Y.-F. Jiang et al. 2016; W. Lu & C. Bonnerot 2020). The blue component of AT 2022cmc's optical/UV light curve indeed shows similar properties to nonjetted TDEs, with a high rest-frame UV luminosity of $\sim 10^{45}$ erg s^{-1} and a blackbody temperature $\sim 3 \times 10^4$ K (I. Andreoni et al. 2022; Y. Yao et al. 2024a).

The follow-up optical spectra of AT 2022cmc, both in the red and blue phases, show a featureless continuum with evidence for host stellar absorption lines but no broad features typically associated with many TDEs. Sw J2058+05 showed a similar lack of features in its optical spectrum (S. B. Cenko et al. 2012; D. R. Pasham et al. 2015). Because of its featureless optical spectra and high peak optical luminosity, I. Andreoni et al. (2022) suggested there may be a connection between jetted TDEs and the featureless class of TDEs put forth by E. Hammerstein et al. (2023a), which show similar high optical luminosities ($M_r \sim -22$ mag). They proposed that TDE-featureless objects may be off-axis jetted TDEs, though current late-time follow-up of TDE-featureless events, particularly in the radio where late-time jet emission can be constrained, is sparse. However, E. Hammerstein et al. (2023b) found that the SMBH at the center of the featureless TDE AT 2020qhs (E. Hammerstein et al. 2023a) is more massive than the canonical "Hills mass", which is the maximum mass that a nonspinning black hole can have in order to disrupt a

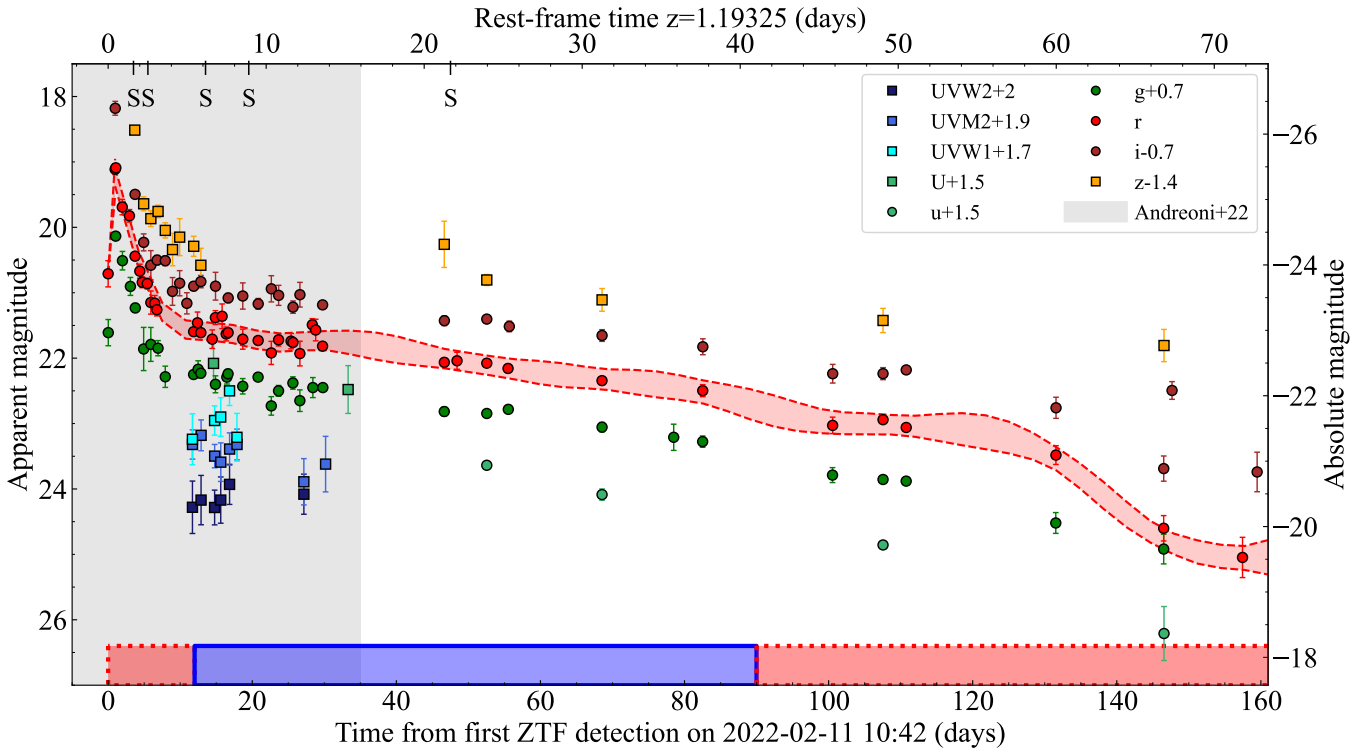

Figure 1. UV and optical light curve of AT 2022cmc in the observed frame. The original discovery light curve published in I. Andreoni et al. (2022) covers the first ∼35 days since discovery (observed frame) and is indicated by the gray shading. Here, we present additional observations that extend the light curve up to ∼160 days since first detection. We show the 1σ band for a Gaussian process regression for the r-band data. Magnitudes are not corrected for Galactic extinction and are not host subtracted because the host is not yet detected in ground-based imaging. We expect the host's contribution to be minimal for the majority of the light curve. Epochs where optical spectra were taken are marked with an "S." On the bottom axis, we note the approximate times of the "red" (dotted border) and "blue" (solid border) phases of the light curve, according to the g–r light curve in Figure 2, with the late-time light curve becoming red once again.

solar-type star outside of the event horizon (J. G. Hills 1975). A high black hole mass could require that the SMBH possesses a spin that would ensure that the tidal radius remains outside the event horizon and produces an observable TDE. If high spin is required to launch a relativistic jet (e.g., A. Tchekhovskoy et al. 2014), this may imply that featureless TDEs are capable of launching jets.

Despite extensive ground-based follow-up observations, the host galaxy of AT 2022cmc has yet to be detected. Limits on the host magnitude were obtained from forced photometry to archival imaging in u and r bands obtained with the Mega-Prime camera on the 3.58 m Canada–France–Hawaii Telescope in 2015 and 2016. These limits are $m_u > 24.19$ mag and $m_r > 24.54$ mag. I. Andreoni et al. (2022) estimated the host properties by modeling the spectral energy distribution (SED). The limits on the galaxy luminosity yielded limits on the host galaxy stellar mass of $\log(M/M_\odot) < 11.2$, which we use as the upper limit in this work. Using these limits on the host, I. Andreoni et al. (2022) put a limit on the SMBH mass of $\log(M/M_{\rm BH}) < 4.7 \times 10^8 M_\odot$. T. Eftekhari et al. (2024) favor lower black hole masses $<10^5 M_\odot$ inferred from the observed X-ray luminosity (assumed to be at the transition between super-Eddington and sub-Eddington) and jet shut-off timescale instead of host galaxy limits. Deep, late-time observations of AT 2022cmc are needed to constrain the host galaxy properties and the properties of the SMBH more strongly.

The discovery of AT 2022cmc, a jetted TDE with a bright optical counterpart, presents an unprecedented opportunity to place this rare class of TDEs in the context of the nonjetted optical TDE population and study the potential connection between TDE-featureless objects and jetted TDEs. We therefore present additional observations of AT 2022cmc at late times to better constrain the thermal component, as well as an analysis of the optical/UV light curve and optical spectra of AT 2022cmc to place it within the context of other optically selected TDEs. This paper is organized as follows. We describe the observations and data reduction in Section 2. In Section 3, we describe the optical spectra fitting methods and light-curve fitting methods we employ. We present the results of both of these in Section 4 and end with a discussion and conclusions in Section 5. Throughout this paper, we adopt a flat cosmology with $\Omega_\Lambda = 0.7$ and $H_0 = 70\,{\rm km\,s^{-1}\,Mpc^{-1}}$ (G. Hinshaw et al. 2013). All magnitudes are reported in the AB system.

2. Data and Observations

2.1. Photometry

Here, we present new observations of AT 2022cmc taken since its discovery on 2022 February 11 10:42:40 UTC (I. Andreoni et al. 2022). In Figure 1, we show the UV/optical light curve including the observations presented in I. Andreoni et al. (2022) which cover up to ∼35 days from the first detection (observed frame). The light curve is characterized by a red color at early times that dominates until ∼12 days (observed frame) and evolves toward a blue ($g - r \lesssim 0$ mag) color (Figure 2). This color persists on the relatively uniform decline until ∼60 days, where the light curve decays more rapidly. We point the reader to I. Andreoni et al. (2022, their

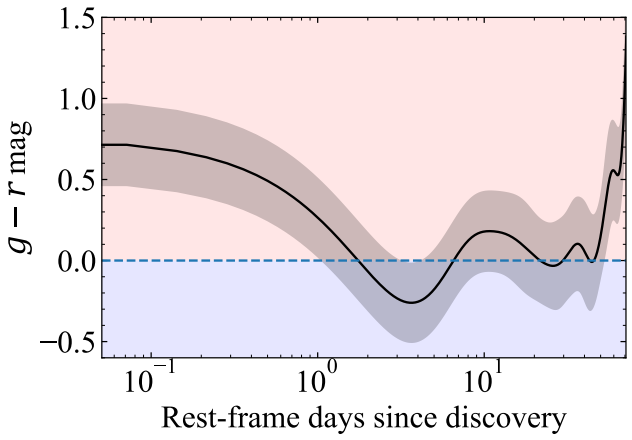

Figure 2. The $g-r$ light curve estimated from Gaussian process regression for both the g and r bands. The shaded region represents the 1σ band and we mark $g-r=0$ with the dashed line. The light curve evolves from red to blue (i.e., $g-r \lesssim 0$) rapidly and remains fairly blue until ∼50 days, after which the light curve significantly reddens. This may be due to a larger host contribution relative to the fading thermal TDE emission at later times. Considering that I. Andreoni et al. (2022) constrained the host emission to $m_r > 24.54$ mag and the r-band light curve drops below this limit around 60 days in the rest frame, this may be plausible.

Section 12) for details on the reduction of the discovery light-curve data.

The additional data that we present here extend the light curve to ∼160 days from the first detection (observed frame) and include observations from the GROWTH India Telescope (GIT; H. Kumar et al. 2022a), the Nordic Optical Telescope (NOT) Alhambra Faint Object Spectrograph and Camera (ALFOSC), Lowell Discovery Telescope (LDT) Large Monolithic Imager (LMI), Large Binocular Telescope (LBT, J. M. Hill et al. 2008) Large Binocular Camera (LBC; R. Speziali et al. 2008), and the Liverpool Telescope (LT) IO:O camera (I. A. Steele et al. 2004). Standard photometric reduction procedures such as bias subtraction, flat-fielding, and cosmic ray rejection were performed on all data.

The GIT photometry was reduced using standard imaging data reduction procedures, including bias correction, flat-fielding, and cosmic ray removal with the `Astro-SCRAPPY` package. Any stacking was performed with `SWarp` (E. Bertin et al. 2002; E. Bertin 2011). Instrumental magnitudes were extracted using PSF photometry and calibrated against the PanSTARRS DR1 catalog, described in H. Kumar et al. (2022b) in detail.

NOT+ALFOSC (Program IDs: 64-501, 64-011, and 65-030 with PIs Sollerman and Charalampopoulos) *gri* observations were reduced with [16] `PyNOT` using standard routines for imaging data. We used aperture photometry to measure the brightness of the transient, which we then calibrated against the brightness of several stars from a cross-matched SDSS catalog.

We reduced the LDT+LMI data using standard data reduction techniques, including bias subtraction, flat-fielding, and cosmic ray rejection. Aperture photometry was computed using `SExtractor` (E. Bertin & S. Arnouts 1996) and calibrated to the PanSTARRS catalog.

LBT+LBC imaging data were reduced using the data reduction pipeline developed at INAF - Osservatorio Astronomico di Roma (A. Fontana et al. 2014) which includes bias subtraction and flat-fielding, bad pixel and cosmic ray masking, astrometric calibration, and coaddition. The astrometry was calibrated against field stars in the GAIA DR3 catalog. PSF photometry was performed using `DAOPHOT` and `APPHOT` under `PyRAF/IRAF` and calibrated against the SDSS catalog.

We performed astrometric alignment and stacking of the LT IO:O observations, with exposures showing major tracking errors or poor transparency due to cloud cover being discarded. We extracted the photometry of the transient using a custom IDL routine using seeing-matched aperture photometry fixed at the transient location which was then calibrated to a set of SDSS secondary standard stars in the field.

2.2. Spectroscopy

I. Andreoni et al. (2022) presented six optical spectra of AT 2022cmc taken over ∼16 days (observed frame), starting from ∼4 days after the first ZTF detection, which we reproduce here (Figure 3). The collection of optical data includes spectra taken with NOT+ALFOSC, Gemini+Gemini Multi-Object Spectrograph (GMOS), Very Large Telescope (VLT) + Xshooter, Keck II+DEep Imaging Multi-Object Spectrograph (DEIMOS), and Keck I+Low Resolution Imaging Spectrometer (LRIS; J. B. Oke et al. 1995). We point the reader to I. Andreoni et al. (2022) for details of the data reduction. Several absorption lines in the VLT+Xshooter spectrum were identified as Al III, Fe II, Mn II, Mg II, Mg I, and Ca II and were used to obtain the source redshift of $z = 1.193$.

We also present here for the first time an additional spectrum taken with Keck I+LRIS (PI: Margutti) on 2022 March 31 14:52:48 UTC, ∼28 days (observed frame) after the last spectrum published by I. Andreoni et al. (2022). The $1''$ slit was used with the 400/3400 grism on the blue side, along with the D560 dichroic and 400/8500 grating on the red side to cover the full optical range, with total exposure times of 1840/1800 s on the blue/red sides, respectively. The data reduction followed the standard procedures outlined by J. M. Silverman et al. (2012).

The spectra cover both the red and blue phases of the optical light curve, and while the spectra remain featureless over all epochs, a clear evolution in the continuum is seen. In Figure 3, we show the six spectra of AT 2022cmc presented in I. Andreoni et al. (2022) and the new LRIS spectrum presented here. In Table 1, we summarize the spectroscopic observations of AT 2022cmc.

3. Analysis

Throughout this paper, we compare the light curve of AT 2022cmc to the light curves of nonjetted TDEs. We draw our comparison sample and light curve data from E. Hammerstein et al. (2023a) and use the light-curve fit parameters presented there. We also fit the spectra of the four TDE-featureless objects in the E. Hammerstein et al. (2023a) sample, using the spectra presented in the appendix of that paper, all of which were observed with the DeVeny spectrograph on the LDT. In Figure 3, we show the optical spectra of the four TDE-featureless objects presented in E. Hammerstein et al. (2023a). We describe the methods used to fit the spectra and light curves in the following sections.

[16] https://github.com/jkrogager/PyNOT

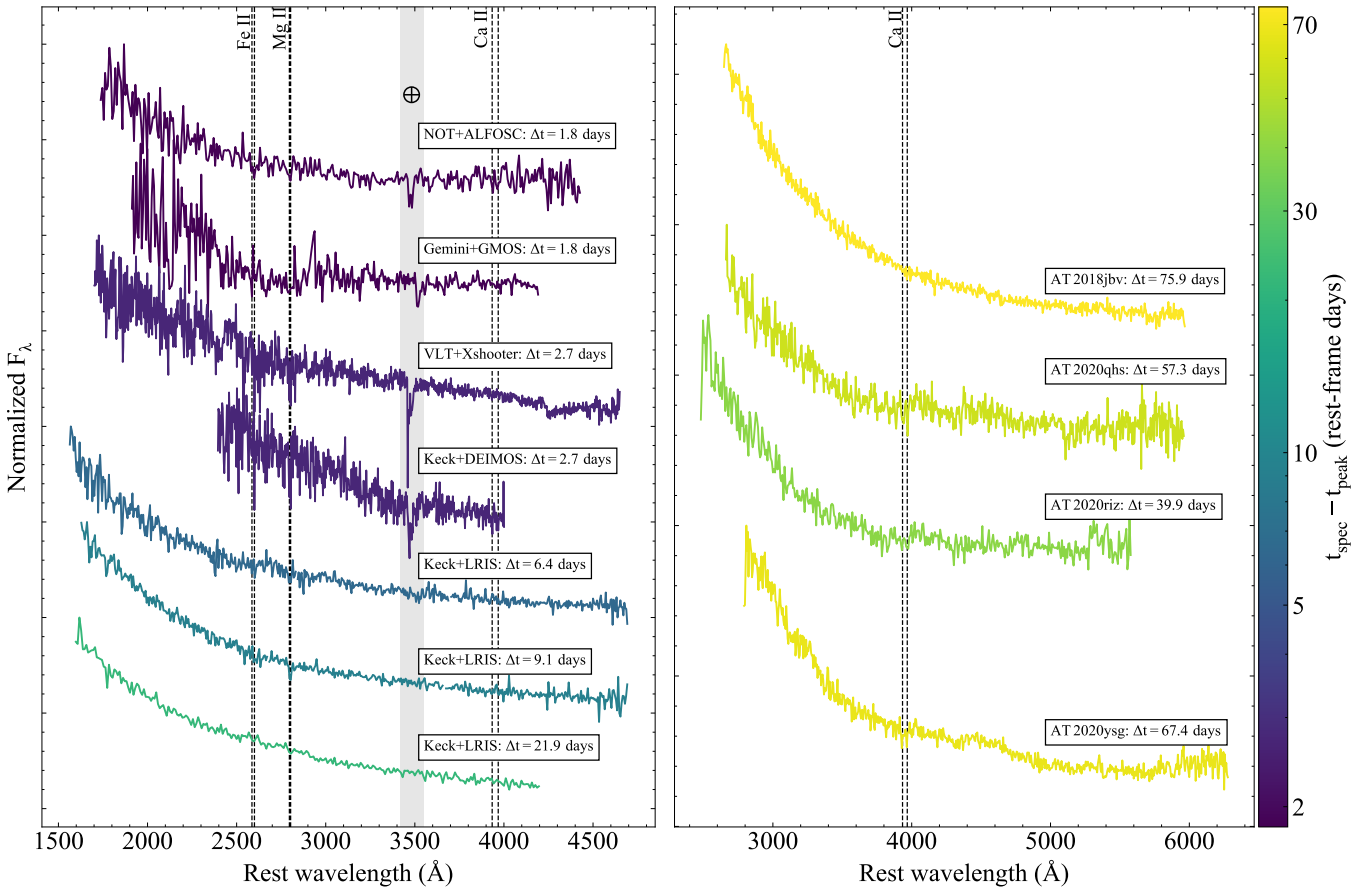

Figure 3. Left: Optical spectra of AT 2022cmc from I. Andreoni et al. (2022) with an additional spectrum from Keck/LRIS at $\Delta t = 21.9$ days (rest frame), presented here for the first time. The spectra cover both the red and blue phases of the light curve, with the red component dominating until ∼5 days rest frame, but remain featureless despite the clear evolution in the continuum. The absorption line near 3500 Å in the AT 2022cmc spectra is telluric (nonastrophysical). Right: Optical spectra of the four TDE-featureless objects in E. Hammerstein et al. (2023a), which show remarkable similarities to the later spectra of AT 2022cmc. The Ca II host stellar absorption feature can be seen. The color of each spectrum corresponds to the approximate phase it was taken relative to peak (or first detection for AT 2022cmc). All spectra have been corrected for Galactic extinction. The AT 2022cmc spectra have been calibrated to the approximate light-curve flux as described in Section 3. Because the TDE-featureless spectra have not been host subtracted, we do not calibrate those to the transient light-curve flux.

Table 1
Summary of Spectroscopic Observations

Name	Redshift	Telescope+Inst.	Date	Phase (Rest-frame Days)
AT 2022cmc	1.193	NOT+ALFOSC	2022 Feb 15	1.8
		Gemini+GMOS	2022 Feb 15	1.8
		VLT+Xshooter	2022 Feb 17	2.7
		Keck II+DEIMOS	2022 Feb 17	2.7
		Keck I+LRIS	2022 Feb 25	6.4
		Keck I+LRIS	2022 Mar 3	9.1
		Keck I+LRIS	2022 Mar 31	21.9
AT 2018jbv	0.340	LDT+DeVeny	2019 Mar 28	75.9
AT 2020qhs	0.345	LDT+DeVeny	2020 Oct 11	57.3
AT 2020riz	0.435	LDT+DeVeny	2020 Oct 15	39.8
AT 2020ysg	0.277	LDT+DeVeny	2021 Jan 11	67.4

Note. Summary of spectroscopic observations for AT 2022cmc and the four TDE-featureless objects in E. Hammerstein et al. (2023a). The first six spectra of AT 2022cmc are from I. Andreoni et al. (2022) and we present an additional late spectrum here. The TDE-featureless objects are taken at much later phases due to the late classification. We include here the redshift, telescope and instrument used, the date the spectrum was taken, and the rest-frame phase (i.e., time relative to flare peak that the observation was taken; we use time since first detection for AT 2022cmc).

3.1. Spectrum Fitting

Given the faintness of the host galaxy ($\gtrsim$24.5 mag, I. Andreoni et al. 2022) and the luminosity of the flare, we expect the optical spectra to be dominated by transient light. It is therefore of interest to characterize the properties of the optical spectra to gain information on the transient itself. While the optical spectra are primarily featureless, the continuum may provide information on the evolution of thermal and nonthermal emission.

Before we perform continuum fitting, we first scale the spectra by the light-curve flux interpolated to the epoch of a

particular spectrum. To do this, we simulate *g*-, *r*-, *i*-, and *z*-band observations from the spectra using `pysynphot` and fit the ratio between this simulated flux and the light-curve flux with a first-order polynomial in order to get a wavelength-dependent correction factor. We note that in some cases (e.g., the DEIMOS spectrum) the spectral coverage only matched the *r* and *i* bands. In contrast to AT 2022cmc, the hosts for the four TDE-featureless events are all detected and may influence the continuum shapes in the spectra. To account for this, we fit these spectra as a linear combination of the model and the host spectrum obtained with stellar population synthesis fits performed in E. Hammerstein et al. (2023a). All spectra have been corrected for Galactic extinction prior to fitting. The spectra of the four featureless TDEs have been corrected for telluric absorption features, while only the Keck+LRIS spectra of AT 2022cmc have been corrected for telluric features.

We fit the continuum of all AT 2022cmc spectra and the four featureless TDEs using two different models. The first model is a blackbody, which allows us to obtain the blackbody temperature and inferred blackbody radius, with the temperature bounds of $[10^4, 10^5]$ K, as is expected for TDEs (e.g., S. van Velzen et al. 2021; E. Hammerstein et al. 2023a). The second model is a power law of the form:

$$F_\nu = F_{\nu,\mathrm{pl}}\left(\frac{\nu}{\nu_0}\right)^{\alpha}, \tag{1}$$

where F_ν is the spectral flux density, F_{pl} is the reference spectral flux density at $\nu_0 = 10^{15}$ Hz, and α is the spectral index. We limit the value of α to $[-5, 5]$ to account for the change in the continuum. Despite the lack of emission and absorption lines in the spectra, apart from some host galaxy stellar absorption lines, we mask regions commonly associated with emission in TDEs (see Section 1) and host stellar absorption lines during the continuum fits in addition to any remaining telluric absorption lines.

For comparison, we also fit the SED from the light curve, which has ugriz coverage beyond what can be supplied by spectroscopy. We fit the same models (a simple power law and blackbody) to bins of 1 day (in the rest frame) which have observations in four unique bands. We describe the results and present the fits in Section 4.

3.2. Light-curve Fitting

For consistency with I. Andreoni et al. (2022), we first fit the AT 2022cmc light curve with a time-evolving power-law spectral component and a *static* blackbody spectral component. In this model, the temperature and luminosity of the blackbody component are constant with time. We note that this model is unlikely to be able to reproduce the light curve at later times once the power-law component has faded. The model is described by

$$L_\nu(t) = L_{\nu_0,\mathrm{peak}}\frac{B_\nu(T_0)}{B_{\nu_0}(T_0)} + L_{\nu,\mathrm{pl}} \times \begin{cases} 10^{\beta_{\mathrm{rise}}(t-t_{\mathrm{peak}})} & t \leqslant t_{\mathrm{peak}} \\ 10^{\beta_{\mathrm{decay}}(t-t_{\mathrm{peak}})} & t > t_{\mathrm{peak}} \end{cases}, \tag{2}$$

where $L_{\nu,\mathrm{pl}}$ describes the power-law component luminosity and is a function of the power-law spectral flux density described by Equation (1) with power-law rise and decay timescales β_{rise} and β_{decay}. Here, ν_0 refers to the reference frequency, which we have chosen to be 10^{15} Hz, and thus $L_{\nu_0,\mathrm{peak}}$ is the luminosity at the time of peak at this frequency. Because I. Andreoni et al. (2022) find little evolution of the power-law spectral index with time, and because we are primarily interested in the properties of the thermal component, we forgo performing a fit with a time-variable power-law spectral index. We limit this fit to the same data as presented in I. Andreoni et al. (2022) instead of using the entire light curve. We will refer to this fit as Model 1.

To compare the UV/optical light curve of AT 2022cmc to the thermal TDEs, we adopt fitting methods similar to S. van Velzen et al. (2021) and E. Hammerstein et al. (2023a). We now include a time-dependent blackbody spectral component which is fitted with a Gaussian rise and an exponential decay. This model is described by

$$L_\nu(t) = L_{\nu,\mathrm{pl}} \times \begin{cases} 10^{\beta_{\mathrm{rise}}(t-t_{\mathrm{peak}})} & t \leqslant t_{\mathrm{peak}} \\ 10^{\beta_{\mathrm{decay}}(t-t_{\mathrm{peak}})} & t > t_{\mathrm{peak}} \end{cases} + L_{\nu_0,\mathrm{peak}}\frac{B_\nu(T_0)}{B_{\nu_0}(T_0)} \times \begin{cases} e^{-(t-t_{\mathrm{peak}})^2/2\sigma^2} & t \leqslant t_{\mathrm{peak}} \\ e^{-(t-t_{\mathrm{peak}})/\tau} & t > t_{\mathrm{peak}} \end{cases}. \tag{3}$$

This model fits for only one temperature, T_0, which is used to predict the luminosity in the other bands as a fraction of the luminosity at the reference frequency. We will refer to this model as Model 2.

Finally, to allow for the most freedom in the evolution of the blackbody component, we perform a third fit similar to Model 2 but with a nonparametric temperature evolution similar to S. van Velzen et al. (2021) and E. Hammerstein et al. (2023a). In this nonparametric temperature model, we fit the temperature at grid points spaced 10 days apart, throwing out grid points without data within 10 days of the point. Since UV coverage is needed to strongly constrain the blackbody peak and is sparse for AT 2022cmc, uncertainties in the temperature for grid points without UV coverage are larger. We will refer to this model as Model 3.

To estimate the parameters of the models above, we use the `emcee` sampler (D. Foreman-Mackey et al. 2013) using a Gaussian likelihood function that includes a "white noise" term, $\ln(f)$, which accounts for any variance in the data not captured by the reported uncertainties and flat priors for all parameters. We use 100 walkers and 4000 steps, discarding the first 2000 steps, which is ~20 times the autocorrelation length, to ensure convergence. The free parameters of the models are listed in Table 2. We have chosen the priors for the power-law component to be consistent with I. Andreoni et al. (2022) but have modified several priors from E. Hammerstein et al. (2023a) for the blackbody component light-curve timescales because we expect them to differ slightly. We assess the quality of our samples by calculating the mean acceptance fraction for each of our models, and find a mean acceptance fraction of ~0.25, which is in the acceptable range for higher dimensional models given by A. Gelman et al. (1996). In summary, we perform the following fits to the AT 2022cmc UV/optical light curve:

Table 2
Light-curve Fit Parameters and Priors

Parameter	Description	Prior
$\log L_{\mathrm{BB},\nu_0}$	Peak blackbody luminosity	$[L_{\max}/2, 2L_{\max}]$
$\log(T_0/\mathrm{K})$	Mean temperature	[4, 5]
$t_{\mathrm{peak,BB}}$	Time of peak	[−2, 20] days
$\log(\sigma_{\mathrm{BB}}/\mathrm{day})$	Gaussian rise time	[0, 1.5]
$\log(\tau_{\mathrm{BB}}/\mathrm{day})$	Exponential decay time	[0, 3]
$\log(F_{\mathrm{peak,pl}}/\mathrm{erg\ s^{-1}\ Hz^{-1}})$	Peak power-law flux density	[10, 80]
α	Power-law spectral index	[−10, 0]
$t_{\mathrm{peak,pl}}$	Time of peak	[−2, 2] days
β_{rise}	Power-law rise time	[0, 100] days
β_{decay}	Power-law decay time	[−100, 0] days
$\ln f$	White noise factor	[−5, −1.8]

Note. The free parameters and corresponding priors for the light-curve analysis described in Section 3.2. $L_{\max}$ is the observed maximum luminosity in any band. The table is split into blackbody parameters (top section) and power-law parameters (middle section).

Model 1. A fit with a time-dependent power-law component (with fixed α) and a static blackbody component described by Equation (2).

Model 2. A fit with a time-dependent power law (with fixed α) and a time-dependent blackbody (with constant temperature) component described by Equation (3).

Model 3. A fit with a time-dependent power law (with fixed α) and a time-dependent blackbody (with nonparametric temperature evolution) component described by Equation (3).

We present the results of this light-curve analysis in Section 4.

We note the steep decline in the light curve at ∼60 days postpeak in the rest frame. To quantify this, we fit a simple broken power law to the $t \geqslant 20$ day light curve in both the g and r bands using `emcee`. The broken power law is of the form:

$$L_\nu(t) = \begin{cases} L_{\nu,\mathrm{break}} \times (t/t_{\mathrm{break}})^{-\alpha_1} & t \leqslant t_{\mathrm{break}} \\ L_{\nu,\mathrm{break}} \times (t/t_{\mathrm{break}})^{-\alpha_2} & t > t_{\mathrm{break}} \end{cases}, \quad (4)$$

where $L_{\nu,\mathrm{break}}$ is the luminosity in the specified band at the break time, t_{break}, and α_1 and α_2 are the power-law indices before and after the break, respectively. We present the results of this fitting in Section 4.

4. Results

4.1. Spectrum Fitting

In Figures 4 and 5, we show the results of the spectrum fitting described in Section 3.1. For each spectrum, the power law and blackbody fits to the continuum are shown, along with the fit parameters. We summarize these in Table 3. The early-time spectra of AT 2022cmc are generally not well-fitted by the blackbody continuum model and in some cases produce temperatures lower and inferred radii larger than the sample of optically discovered thermal TDEs (e.g., S. van Velzen et al. 2021; E. Hammerstein et al. 2023a; Y. Yao et al. 2023). The early-time emission is described much better by the power-law fits to the continuum, which is unsurprising given that the red component dominates the light curve until ∼12 days (observed frame) from the first detection (I. Andreoni et al. 2022). The blackbody continuum fits to the later spectra taken with LRIS produce more reasonable results (i.e., those expected for TDEs) with regard to blackbody temperature and inferred radius. The spectra show remarkable similarity to the featureless TDEs (shown in the bottom 4 panels of Figure 4).

While the single model continuum fits cannot completely capture the nature of the continuum emission, the change in the power-law spectral index α is evident from these fits. In Figure 6, we show the power-law spectral index α and the blackbody temperature for each spectrum as well as from the SED, which covers a larger range in time. The evolution from $\alpha = -0.74$ to $\alpha = 0.46$ is expected as the red, nonthermal component of the SED quickly fades in the first ∼10 days of the transient. Interestingly, the power-law index evolves back toward values less than zero after ∼30 days. Whether this is intrinsic evolution of the transient or is related to a larger fraction of the light being related to the host is difficult to determine without strong host constraints.

4.2. Light-curve Fitting

In Table 4, we show the results from fitting the three models described in Section 3.2 to the UV/optical light curve of AT 2022cmc. For the time-dependent power-law and static blackbody fit (Model 1), we find results consistent with the light-curve fit performed by I. Andreoni et al. (2022). While the blackbody luminosity we find is lower ($L_{\mathrm{BB}} = 10^{44.41}$ erg s^{-1} compared to $L_{\mathrm{BB}} = 10^{45.53}$ erg s^{-1}) and the blackbody temperature is higher ($T_{\mathrm{BB}} = 10^{4.53}$ K compared to $T_{\mathrm{BB}} = 10^{4.48}$ K), our results are nonetheless consistent with typical values for TDEs. The time-dependent power-law component is consistent within uncertainties with the findings of I. Andreoni et al. (2022), with the reference spectral flux density $F_{\mathrm{peak,pl}} = 10^{30.59}$ erg s^{-1} Hz^{-1} compared to their $F_{\mathrm{peak,pl}} = 10^{30.51}$ erg s^{-1} Hz^{-1}, and the spectral index $\alpha = -1.30$ compared to their $\alpha = -1.32$.[17] When we allow the blackbody luminosity to vary with time, our results for both the power-law and blackbody components are consistent within mutual uncertainties. The Model 3 fits, where the temperature is allowed to evolve over the course of the light curve, produce only marginally different results, all but the power-law component rise time consistent within uncertainties. This is likely due to the lack of data on the rise of the light curve and the rapid nature of the rise. We show the light curve fits to only the r-band light curve (for clarity) in Figure 7.

In Figure 8, we show the SED derived from all fits, starting from the peak of the light curve until ∼60 days postpeak (rest frame). There is a clear evolution in the shape of the SED in all cases, with the early-time SED dominated by the power-law component until ∼6 days postpeak. This is consistent with I. Andreoni et al. (2022). The blackbody component is found to peak ∼5 days after the power-law component. Similar behavior is observed in the continuum in the optical spectra.

In Figure 9, we show the evolution of the blackbody temperature from Model 3. E. Hammerstein et al. (2023a) found that the blackbody temperature of the thermal TDEs is largely constant or even increasing, while the temperature of AT 2022cmc appears to decrease. We note that there are very limited UV observations of AT 2022cmc, which are needed to

[17] Note that I. Andreoni et al. (2022) label the power-law spectral index as β.

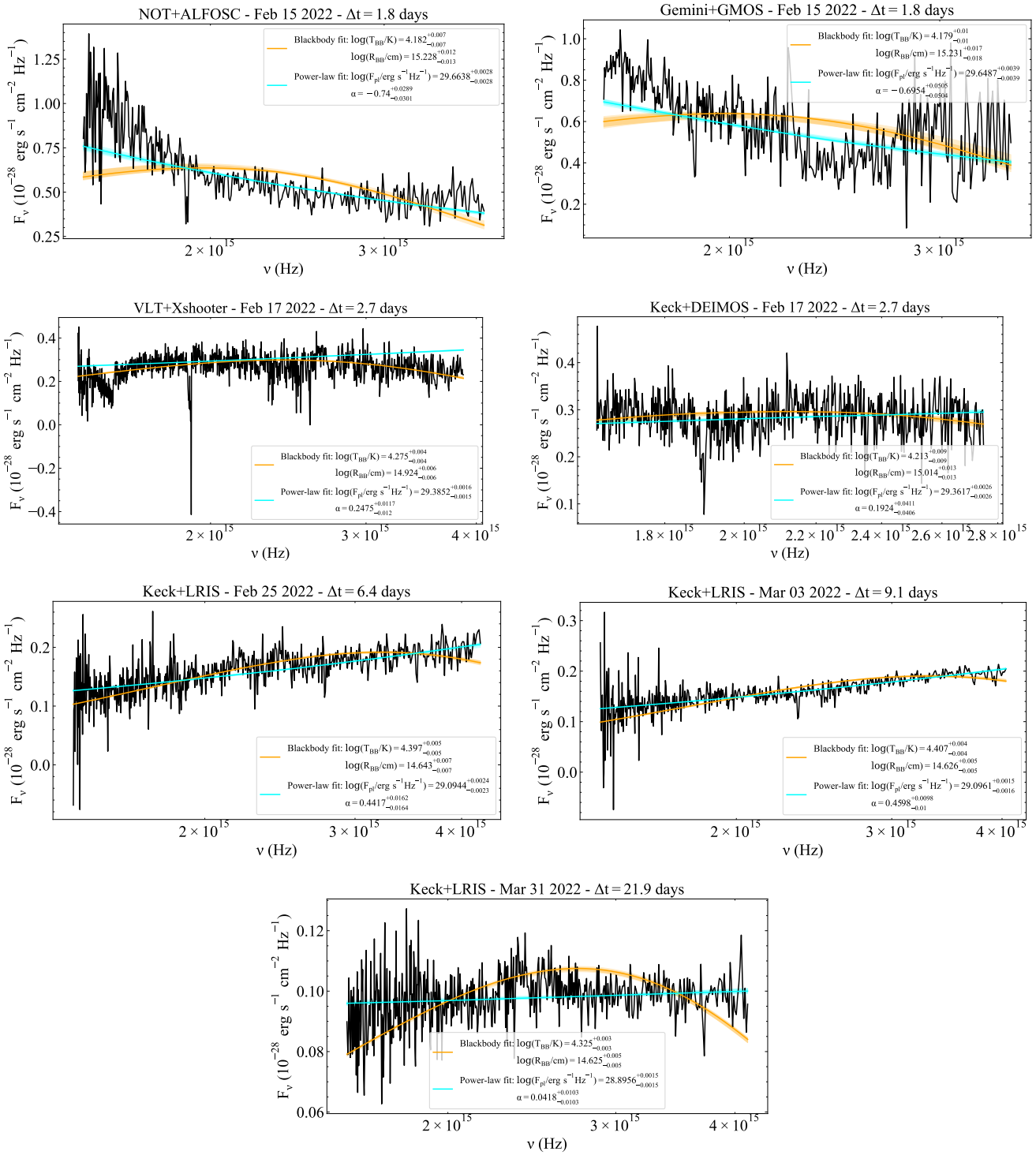

Figure 4. The blackbody (orange line) and power-law (blue line) fits for AT 2022cmc described in Section 3.1. The early-time ($\Delta t \lesssim 2$ days) AT 2022cmc spectra are well-described by a red power-law continuum, consistent with the red phase of the light curve, while the late-time ($\Delta t \gtrsim 6$ days) spectra are more consistent with a bluer continuum as expected in the blue phase of the light curve. The change in the continuum from 2022 March 3 to 2022 March 31 is also seen in the light curve, where the SED begins to redden once again and may either be intrinsic transient evolution or related to a greater fractional contribution from the host at later times. We note that for the later epochs, while the power law may provide a better overall fit, the power-law spectral index is inconsistent with that of the red phase of the light curve (i.e., $\alpha > 0$ instead of $\alpha < 0$ in the red phase). The absorption features below 2×10^{15} Hz are telluric features which are masked during fitting. Shading for each line corresponds to 1σ (darker shading) and 3σ (lighter shading) bands. All spectra are in the rest frame. Fit parameters are listed in Table 3.

strongly constrain the peak of the blackbody SED. In the next section, we compare the blackbody component of the fit to other TDEs discovered in the optical.

In Table 5, we present the results of the broken power-law fit to the $t \geqslant 20$ day light curve. There is generally good agreement between the r and g bands for both the break time and power-law indices. Both bands imply a break in the light curve at $\sim$52 days. We note the large uncertainties on the α_2 power-law index, which is only constrained by a few data points.

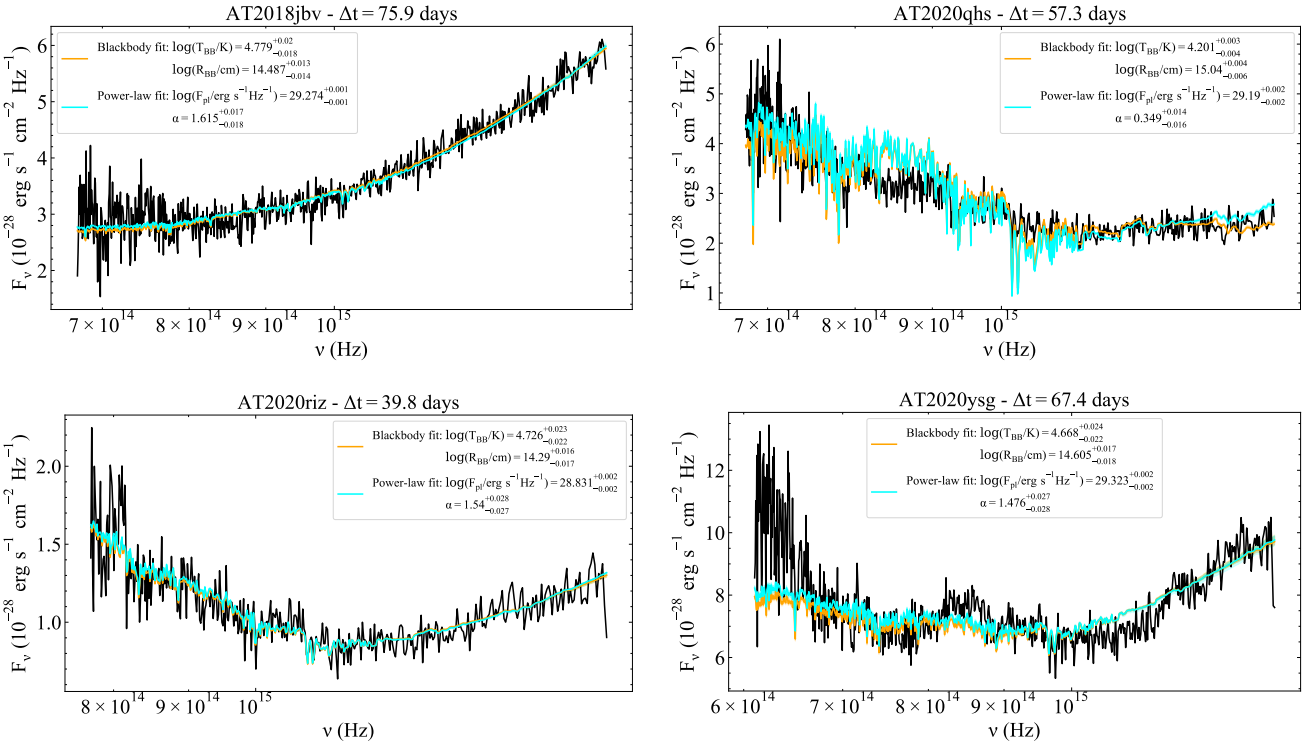

Figure 5. The blackbody (orange line) and power-law (blue line) fits for the featureless TDEs from E. Hammerstein et al. (2023a), including contribution from the host SED. The power-law fits are mostly inconsistent with the nonthermal emission that is seen for AT 2022cmc, in that they correspond to positive α values (i.e., bluer) while early spectroscopy of AT 2022cmc shows negative α values (i.e., redder). Nonetheless, the continuum shapes, particularly in AT 2018jbv, are reminiscent of the later, blue phase AT 2022cmc spectra. Shading for each line corresponds to 1σ (darker shading) and 3σ (lighter shading) bands. For AT 2020ysg, we note the bump between 8 and 9 $\times$ 10^{14} Hz, which may correspond to the He II λ3203 line. All spectra are in the rest frame. Fit parameters are listed in Table 3.

Table 3
Results from Spectrum Fitting

Name	Telescope/Inst.	Phase (days)	$\log(F_{\rm pl}/{\rm erg\ s^{-1}\ Hz^{-1}})$	α	$\log(T_{\rm BB}/{\rm K})$	$\log(R_{\rm BB}/{\rm cm})$
AT 2022cmc	NOT+ALFOSC	1.8	29.664 ± 0.003	−0.74 ± 0.03	4.182 ± 0.007	15.228 ± 0.012
	Gemini+GMOS	1.8	29.649 ± 0.004	−0.69 ± 0.05	4.179 ± 0.01	15.231 ± 0.017
	VLT+Xshooter	2.7	29.385 ± 0.002	0.25 ± 0.01	4.275 ± 0.004	14.924 ± 0.006
	Keck+DEIMOS	2.7	29.362 ± 0.003	0.19 ± 0.04	4.213 ± 0.009	15.014 ± 0.013
	Keck+LRIS	6.4	29.094 ± 0.002	0.44 ± 0.02	4.397 ± 0.005	14.643 ± 0.007
	Keck+LRIS	9.1	29.096 ± 0.002	0.46 ± 0.01	4.407 ± 0.004	14.626 ± 0.005
	Keck+LRIS	21.9	8.896 ± 0.002	0.04 ± 0.01	4.325 ± 0.003	14.625 ± 0.005
AT 2018jbv	LDT+DeVeny	75.9	29.274 ± 0.001	1.62 ± 0.02	4.779 ± 0.020	14.487 ± 0.013
AT 2020qhs	LDT+DeVeny	57.3	29.190 ± 0.002	0.35 ± 0.01	4.201 ± 0.003	15.040 ± 0.004
AT 2020riz	LDT+DeVeny	39.8	28.831 ± 0.002	1.54 ± 0.03	4.726 ± 0.023	14.290 ± 0.016
AT 2020ysg	LDT+DeVeny	67.4	29.323 ± 0.002	1.48 ± 0.03	4.668 ± 0.024	14.605 ± 0.017

Note. Results from power-law and blackbody continuum fits to optical spectra. The power-law spectral index α for AT 2022cmc begins negative and corresponds to the red component of the light curve in Figures 2 and 6. Notably, α begins to transition back toward zero in the latest epoch. This trend is seen in the late-time light-curve epochs until ∼60 days. The nature of this evolution is unusual for a TDE and may be related to a greater fractional host component at later times.

5. Discussion

Several correlations have been found between properties of optical TDE light curves as well as between these properties and the SMBH mass (or host galaxy mass as a proxy). S. van Velzen et al. (2021) found that the rise time of the flare ($\sigma_{\rm BB}$) is correlated with the peak bolometric luminosity. This correlation was not found by E. Hammerstein et al. (2023a), but their smaller sample size may affect this conclusion. E. Hammerstein et al. (2023a) did, however, find a weak correlation between the decay timescale and the peak luminosity, which has also been found by J. T. Hinkle et al. (2020). S. van Velzen et al. (2021) also reported a positive correlation between the decay timescale ($\tau_{\rm BB}$) for their sample of TDEs and the host galaxy stellar mass. This correlation was also found in the E. Hammerstein et al. (2023a) sample, in addition to a correlation with the rise time, and a similar correlation was confirmed by Y. Yao et al. (2023). If the thermal, blue component in AT 2022cmc arises in the same way as for thermal TDEs, we might expect that it falls in line with these same correlations. In this section, we compare the properties of the UV/optical emission in AT 2022cmc to those of optically selected thermal TDEs, focusing on properties for which significant correlations have been reported. We use

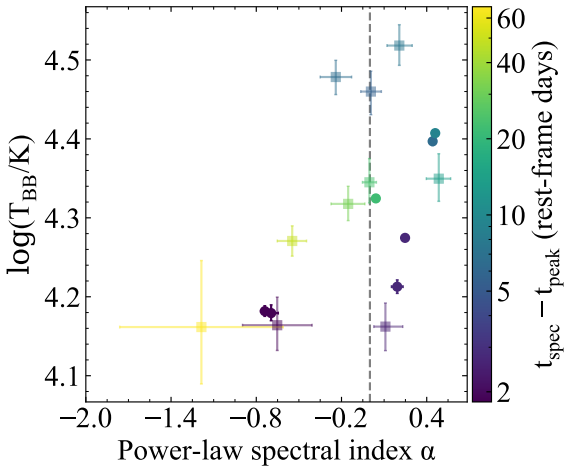

Figure 6. The evolution of the blackbody temperature $T_{\rm BB}$ and the power-law spectral index α from the spectrum continuum fits (circles). We also show the results from fitting the SED derived from the photometry (squares). There is a clear evolution in the power-law spectral index due to the fading of the red, nonthermal component in AT 2022cmc after ∼12 days, where the blue, thermal component takes over. This is also evident in the fits to the SED. We note that the single model continuum fits (either power law or blackbody) cannot fully capture the nature of the emission, but provide evidence for the clear evolution of the source emission in its red and blue phases. We denote $\alpha = 0$ with the dashed gray line, negative and positive values of which roughly coincide with the red and blue phases of the light curves, respectively.

Table 4
Results from Fits to AT 2022cmc Optical Light Curve

Parameter	Model 1	Model 2	Model 3
$\log(L_{\rm BB,\nu_0}/{\rm erg\ s^{-1}})$	$44.41^{+0.09}_{-0.12}$	$44.46^{+0.14}_{-0.14}$	$44.41^{+0.12}_{-0.13}$
$t_{\rm peak,BB}$ (day)[a]	⋯	$2.78^{+8.37}_{-3.36}$	$5.84^{+7.80}_{-5.46}$
$\log(\sigma_{\rm BB}/{\rm day})$	⋯	$1.06^{+0.31}_{-0.58}$	$1.06^{+0.31}_{-0.48}$
$\log(\tau_{\rm BB}/{\rm day})$	⋯	$1.48^{+0.48}_{-0.29}$	$1.53^{+0.59}_{-0.40}$
$\log(T_0/{\rm K})$	$4.53^{+0.07}_{-0.06}$	$4.53^{+0.08}_{-0.07}$	$4.57^{+0.27}_{-0.27}$
$\log(F_{\rm peak,pl}/{\rm erg\ s^{-1}\ Hz^{-1}})$	$30.59^{+0.07}_{-0.07}$	$30.59^{+0.07}_{-0.07}$	$30.56^{+0.06}_{-0.05}$
$t_{\rm peak,PL}$ (day)[a]	$-0.02^{+0.15}_{-0.14}$	$-0.02^{+0.14}_{-0.15}$	$0.03^{+0.15}_{-0.14}$
$\beta_{\rm rise}$ (day)	$50.43^{+33.61}_{-35.01}$	$46.40^{+34.34}_{-33.32}$	$3.62^{+2.85}_{-1.72}$
$\beta_{\rm decay}$ (day)	$-0.47^{+0.05}_{-0.06}$	$-0.47^{+0.06}_{-0.08}$	$-0.46^{+0.06}_{-0.07}$
α	$-1.30^{+0.39}_{-0.41}$	$-1.31^{+0.42}_{-0.51}$	$-1.11^{+0.41}_{-0.44}$

Notes. Results from fits to AT 2022cmc optical light curve. The fit numbers correspond to those in Section 3.2.
[a] Rest frame, with respect to maximum light.

the sample of 30 TDEs from ZTF for comparison (E. Hammerstein et al. 2023a).

In Figure 10, we show the light-curve parameters $\sigma_{\rm BB}$, $\tau_{\rm BB}$, peak bolometric blackbody luminosity $L_{\rm peak,BB}$ calculated using the mean blackbody temperature T_0 as a function of the host galaxy stellar mass for the 30 TDEs and AT 2022cmc obtained from Model 2 (Section 3.2). While black hole mass estimates are available for some objects in the comparison sample (e.g., E. Hammerstein et al. 2023b; Y. Yao et al. 2023), we choose the host galaxy stellar mass for consistency across all objects. Additionally, E. Hammerstein et al. (2023b) and Y. Yao et al. (2023) find that the host galaxy stellar mass is strongly correlated with the black hole mass derived from stellar kinematics. We adopt the estimate from I. Andreoni et al. (2022) for the upper limit on the host stellar mass of $\log(M_{\rm gal}/M_\odot) < 11.2$. We emphasize that this is only an upper limit on the host galaxy

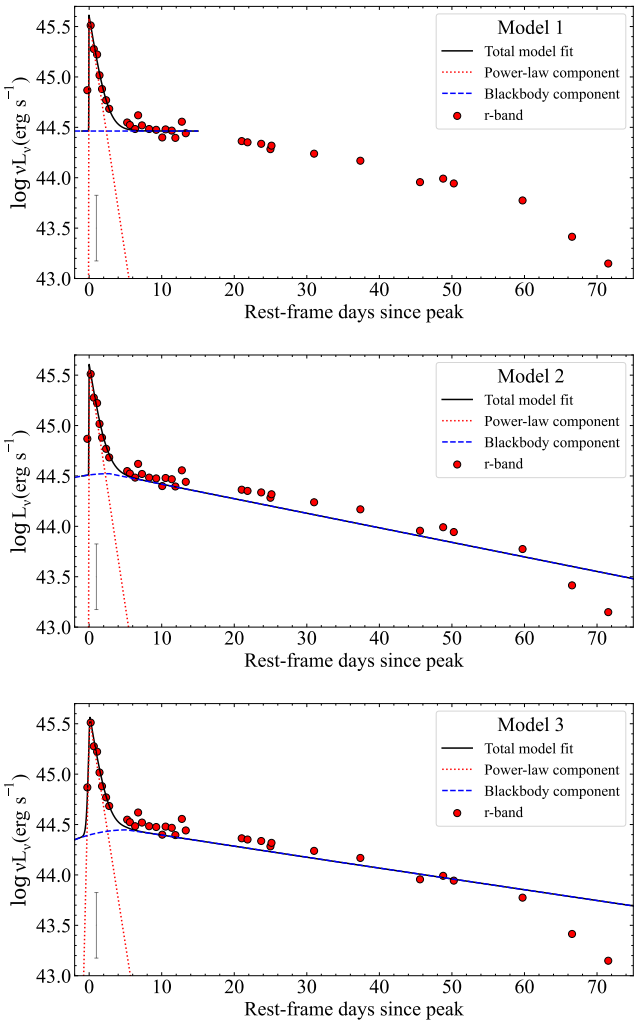

Figure 7. Model fits to the AT 2022cmc light curve, showing only the r band for clarity. For each fit we show the two components, the power-law and the blackbody as red dotted and blue dashed lines, respectively. The rise times for the two components, $\sigma_{\rm BB}$ and $\beta_{\rm rise}$, are derived from the red and blue curves. We note that the rise times, particularly for the power-law component, are not well constrained. Additionally, we show the median uncertainties on the light-curve data points in the bottom left corner. The Model 1 fit is limited to the first ∼15 days to match I. Andreoni et al. (2022). We note the unusual accelerated decay after ∼60 days, which is uncommon in thermal TDEs.

mass and may change once better constraints are placed on the host galaxy's properties in future observations.

While both the rise and decay timescales for AT 2022cmc are faster than would normally be expected for a TDE if the host galaxy mass is at the upper limit, this may not be surprising given the light curve and difficulty in constraining a sparsely sampled rise and fast evolving transient. Both the rise and decay timescales are still comparable to other thermal TDEs, albeit for much lower host galaxy masses. Further host characterization will confirm whether AT 2022cmc aligns with these correlations. The values for the other parameters (peak bolometric luminosity, and blackbody temperature) are more consistent with previously found correlations.

Interestingly, the values for the peak bolometric luminosity and blackbody temperature show remarkable similarity to the TDE-featureless class. I. Andreoni et al. (2022) noted the potential connection between AT 2022cmc and the TDE-featureless class due to similarities in photometric and spectroscopic properties, such as peak luminosity and lack of broad

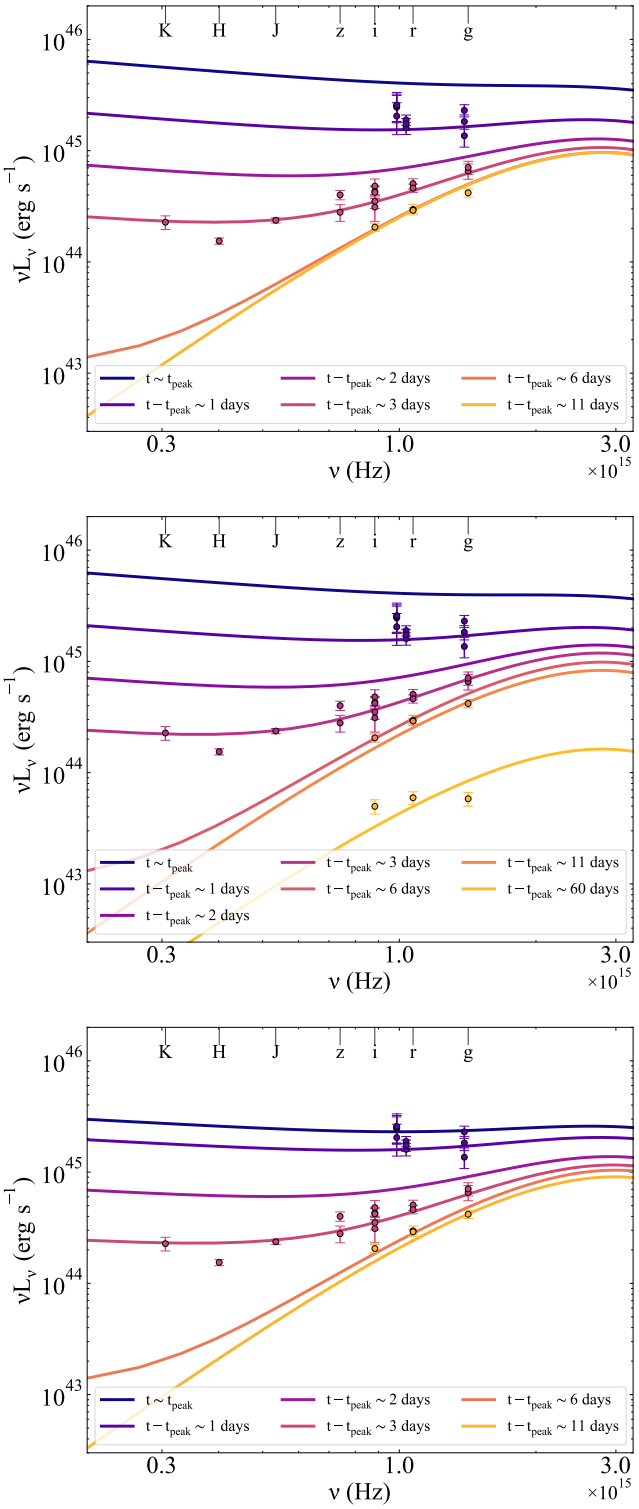

Figure 8. Evolution of the SED starting from peak ($t = t_{peak}$) until the ∼last epoch of observations (rest frame) in order of Model 1 (top), Model 2 (middle), and Model 3 (bottom). For each panel, we show light-curve data points for t–$t_{peak} \approx 1, 3, 11, 60$ days. All SEDs are in the rest frame.

lines in the optical spectra. They suggest that the TDE-featureless class may represent the off-axis jetted TDE scenario. This connection is potentially further supported due to the high black hole masses observed for TDE-featureless objects, which could necessitate a non-negligible spin for the black holes in these events so that the stars are disrupted outside of

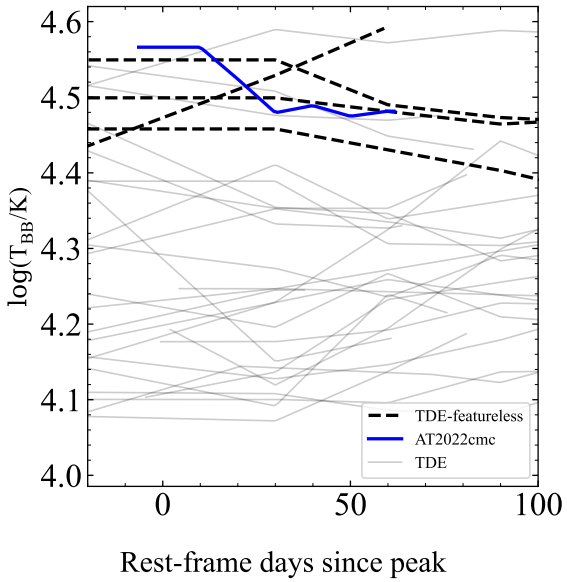

Figure 9. Evolution of the blackbody temperature from Model 3 with AT 2022cmc represented by the solid blue line, the featureless TDEs represented by the dashed black lines, and other thermal TDEs as the gray solid lines. The thermal TDEs and the featureless TDEs show a variety of behaviors, although the majority show a near constant or increasing temperature (E. Hammerstein et al. 2023a). AT 2022cmc appears to decrease in temperature, but the late-time temperature is not well constrained without UV observations.

Table 5
Results from Broken Power-law Fits

Parameter	r Band	g Band
$\log L_{\nu,\mathrm{break}}$	$43.92^{+0.57}_{-0.31}$	$44.01^{+0.52}_{-0.31}$
t_{break}	$51.78^{+11.02}_{-8.77}$	$51.87^{+11.98}_{-8.51}$
α_1	$0.92^{+1.21}_{-0.66}$	$1.00^{+1.15}_{-0.71}$
α_2	$5.38^{+3.20}_{-3.56}$	$5.13^{+3.25}_{-3.58}$

Note. Results from broken power-law fits to AT 2022cmc r- and g-band light curves. t_{break} is measured in the rest frame with respect to the time of first detection. We note the large uncertainties on the α_2 values, which are only constrained by a few data points.

the event horizon, depending on the type of star that is disrupted. E. Hammerstein et al. (2023b) reported a mass of $\log(M_{\mathrm{BH}}/M_\odot) = 8.01 \pm 0.82$ obtained from stellar kinematics for AT 2020qhs. Additional measurements made by Y. Yao et al. (2023) for featureless events yielded masses $\log(M_{\mathrm{BH}}/M_\odot) = 7.16 - 8.23$. A. Mummery et al. (2024) found that the black hole masses inferred from the late-time light-curve plateaus of TDE-featureless events strongly imply non-negligible spin parameters. If high spin is required to launch a relativistic jet (e.g., A. Tchekhovskoy et al. 2014; I. Andreoni et al. 2022), then the TDE-featureless class may be capable of launching relativistic jets. This should be interpreted cautiously, however, because TDEs around SMBHs with masses lower than $\sim 10^8 M_\odot$ (the "Hills mass") may still have large spins and SMBHs above $\sim 10^8 M_\odot$ can disrupt nonsolar type stars outside of the event horizon.

A high black hole mass for jetted events would be in contrast to the findings of T. Eftekhari et al. (2024), which disfavored larger black holes for producing jets in TDEs and concluded that jetted TDEs may preferentially come from lower mass SMBHs as a result of lower jet and higher disk efficiencies at higher

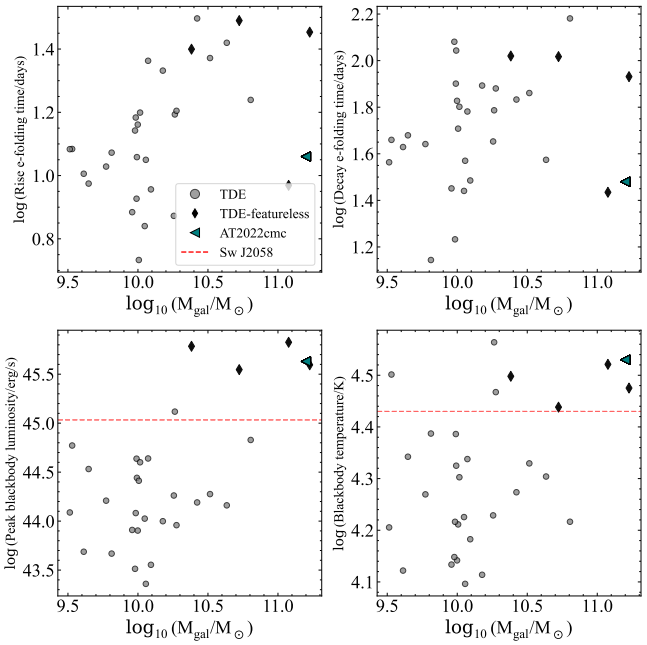

Figure 10. Selected light-curve parameters from Model 1 for the 30 TDEs from ZTF (gray circles, black diamonds indicate TDE-featureless; E. Hammerstein et al. 2023a) and AT 2022cmc (blue triangle). The rise and decay times for the blackbody component are much shorter for AT 2022cmc than for the other TDEs. The peak bolometric blackbody luminosity and mean blackbody temperature are more consistent with expected values from TDEs and show remarkable similarity to the TDE-featureless class.

black hole masses. T. Eftekhari et al. (2024) also found evidence for the cessation of jet activity in the late-time X-ray light curve of AT 2022cmc, which occurred at $t_{\rm rest} \approx 98$ days. In the optical light curve, we see an unusual steepening in the decay rate approximately 40 days prior to the X-ray break. Our broken power-law fits to the *r*- and *g*-band light curves constrain the time between the optical break and the X-ray break to be ∼46 days. T. Eftekhari et al. (2024) attribute the sudden drop in X-ray emission to an accretion state transition which subsequently manifests as a jet shut-off. The break in the optical light curve prior to the cessation of the jet may imply that the origin of the optical emission is in fact related to the accretion flow or reprocessing of emission related to the accretion flow. However, it is difficult to discern whether the peculiar late-time evolution of the optical light curve is related to the intrinsic evolution of the transient, particularly given the reddening of the SED after ∼50 days.

The reddening in the light curve and evolution of the power-law spectral index at late times is puzzling. Previous studies of TDEs have found that, in general, reddening is not observed (S. van Velzen et al. 2021; E. Hammerstein et al. 2023a). This reddening could be due to higher host contribution at late times. The host galaxy limit in the *r* band is at $m_{\rm r} > 24.54$ mag. This does not dominate the light curve until ∼64 days postpeak (rest frame) but could contribute significantly at earlier times if this limit is taken as approximately true. At the flip from red to blue at ∼50 days postpeak (rest frame), the host could contribute up to 25% of the flux in the *r* band. At earlier times, closer to the power-law index change around ∼22 days postpeak (rest frame), the host may contribute up to 10% of the flux in the *r* band. Without a true understanding of the host SED, it is difficult to say the degree to which the other bands might be affected and how that might affect the SED shape. However, if the host galaxy of AT 2022cmc is similar to those of other featureless TDEs (e.g., Figure 5), the red host can contribute significantly to the red filters. We also note that the jetted TDE Sw J2058+05 also showed evolution in the thermal component, which became significantly cooler prior to the drop in the X-ray flux (D. R. Pasham et al. 2015).

Two other jetted TDE candidates exhibited faint optical counterparts: Sw J2058+05 (S. B. Cenko et al. 2012; D. R. Pasham et al. 2015) and Sw J1112-82 (G. C. Brown et al. 2015, 2017). D. R. Pasham et al. (2015) fit the UV/optical observations of Sw J2058+05, which also showed a featureless optical spectrum, with a single blackbody model, yielding a mean temperature over several epochs of $T_{\rm BB} = 10^{4.43}$ K. This is comparable to AT 2022cmc and the TDE-featureless objects. The peak bolometric luminosity implied by the UV/optical observations is also comparable to AT 2022cmc and the TDE-featureless class at $L_{\rm BB} = 10^{45.03}$ erg s^{-1}. We show this limit in Figure 10. Black hole mass estimates from host galaxy properties for both of these events are significantly lower than estimates for the mass in AT 2022cmc from host galaxy properties (D. R. Pasham et al. 2015; G. C. Brown et al. 2017; I. Andreoni et al. 2022). Given that we have only an upper limit on the host galaxy mass for AT 2022cmc, there may not be any discrepancy. Additionally, by modeling the X-ray light curve, T. Eftekhari et al. (2024) found that lower black hole masses are favored for Sw J2058+05, similar to AT 2022cmc. As more jetted TDEs are discovered and their host galaxies are characterized, we can further explore the similarities and differences between the optical components in jetted TDEs and the TDE-featureless class.

Observations of TDE-featureless objects that may indicate the presence of a jet, such as late-time radio emission, have yet to be published. Y. Cendes et al. (2024) found that ∼40% of optical TDEs are detected at late times in the radio, but concluded that this emission is likely due to outflows instead of off-axis relativistic jets. It is clear that future and long-term follow-up observations of TDE-featureless events are needed to further explore this possible connection. Interestingly, the rate of "overluminous" TDEs (i.e., $M_r < -20.5$ mag, which includes both jetted TDEs and featureless TDEs) is $2\,{\rm Gpc^{-1}\,yr^{-1}}$ (integrated from the luminosity function in Y. Yao et al. 2023), which is roughly consistent with the estimate from I. Andreoni et al. (2022) that ∼1% of all TDEs produce relativistic jets.

Additionally, spectral sequences of featureless TDEs from at or near peak to postpeak are available for only one event (see Figure 7 of Y. Yao et al. 2023), as are spectra outside of the rest-frame optical band. J. Guillochon et al. (2014) showed that for PS1-10jh, the lines of Hα, Hβ, and He I were not visible at early times because of the intensity of the hydrogen-ionizing flux, but may have become visible at later times as the event faded. Due to their high luminosities, this may be a plausible explanation for the featureless nature of jetted and TDE-featureless spectra, as well as for their high temperatures. Therefore, it may not be required that TDE-featureless events are also jetted but are connected to jetted TDEs by luminosity alone. This could also explain the higher luminosities of some TDE-He events (e.g., E. Hammerstein et al. 2023a).

If the two classes are similar only in luminosity, and TDE-featureless are not off-axis analogs to jetted TDEs, then the question becomes: how can we get such a luminous flare around a very massive black hole? Since the fallback timescale is proportional to black hole mass as $t_{\rm fb} \propto M_{\rm BH}^{1/2}$ and the fallback rate is $\dot{M}_{\rm fb} \propto M_*/(3t_{\rm fb})$ (where M_* is the mass of the disrupted star), for the same star, a higher black hole mass will have a lower

accretion rate and therefore a lower luminosity. One way to increase the luminosity in these featureless, overluminous events is to increase the amount of mass accreted. This can be done through the disruption of very massive stars. However, given that the host galaxies of featureless TDEs are red, quiescent galaxies (E. Hammerstein et al. 2023a), the presence of young, massive stars available for disruption is unlikely. Another way to increase the luminosity is to increase the radiative efficiency. M. Nicholl et al. (2022) showed that there may be a positive correlation between black hole mass and radiative efficiency. Interestingly, efficiency is linked with the spin alignment of the black hole, with greater efficiency tied to larger spin magnitudes and prograde orbits (e.g., P. G. Jonker et al. 2020). This could imply that more massive objects are rotating more rapidly, as suggested by E. Hammerstein et al. (2023b).

Host galaxy characterization of jetted TDEs will help to confirm a link to featureless thermal TDEs, whose hosts are typically more massive and redder than other types of thermal TDEs (E. Hammerstein et al. 2023a; Y. Yao et al. 2023). Finally, the lack of jet-associated emission observed at late times in TDE-featureless events (e.g., Y. Yao et al. 2025), particularly over-massive events that could have high spin, may indicate that higher spin alone is not sufficient to produce jets in TDEs.

We have shown here that the thermal component present in the UV/optical light curve of AT 2022cmc is indeed comparable to the light curves of other TDEs which are dominated by almost exclusively thermal emission. Moreover, we have shown that the properties of the thermal component are similar to the class of featureless TDEs put forth by E. Hammerstein et al. (2023a). Future studies (e.g., Y. Yao et al. 2025) will need to investigate the presence of emission that might indicate that these TDE-featureless objects are indeed off-axis analogs to jetted TDEs, as well as the appearance of line features in these events at late times.

Acknowledgments

We thank the reviewer for the helpful comments toward improving this manuscript. Portions of this work served as a chapter in E.H.'s dissertation. This material is based upon work supported by NASA under award No. 80GSFC21M0002. The TReX team at UC Berkeley is partially funded by the National Science Foundation under award No. AST-2224255. A.R. acknowledges INAF project Supporto Arizona & Italia.

Based on observations made with the Nordic Optical Telescope, owned in collaboration by the University of Turku and Aarhus University, and operated jointly by Aarhus University, the University of Turku, and the University of Oslo, representing Denmark, Finland, and Norway, the University of Iceland and Stockholm University at the Observatorio del Roque de los Muchachos, La Palma, Spain, of the Instituto de Astrofisica de Canarias. The GROWTH India Telescope (GIT) is a 70 cm telescope with a $0.^{\circ}7$ field of view set up by the Indian Institute of Astrophysics (IIA) and the Indian Institute of Technology Bombay (IITB) with funding from Indo-US Science and Technology Forum and the Science and Engineering Research Board, Department of Science and Technology, Government of India. It is located at the Indian Astronomical Observatory (IAO, Hanle). We acknowledge funding by the IITB alumni batch of 1994, which partially supports the operation of the telescope. The LBT is an international collaboration of the University of Arizona, Italy (INAF: Istituto Nazionale di Astrofisica), Germany (LBTB: LBT Beteiligungsgesellschaft), The Ohio State University, representing also the University of Minnesota, the University of Virginia, and the University of Notre Dame.

Appendix
AT 2022cmc Light Curve

In Table 6, we present the new observations of AT 2022cmc since its discovery in I. Andreoni et al. (2022). We note that all observations use the SDSS photometric system, which exhibits

Table 6
New Observations of AT 2022cmc

MJD	Filter	Mag	eMag	Instrument
59669.87	*r*	22.04	0.11	GITCamera
59676.79	*r*	22.21	0.1	GITCamera
59676.87	*g*	22.02	0.11	GITCamera
59677.1	*g*	22.11	0.06	ALFOSC
59677.11	*r*	22.12	0.06	ALFOSC
59677.13	*i*	22.22	0.07	ALFOSC
59689.98	*r*	22.28	0.16	IO:O
59699.95	*g*	22.51	0.17	IO:O
59703.96	*g*	22.58	0.07	ALFOSC
59703.97	*r*	22.5	0.08	ALFOSC
59703.99	*i*	22.53	0.1	ALFOSC
59721.99	*g*	23.09	0.1	ALFOSC
59722.0	*r*	23.03	0.11	ALFOSC
59722.02	*i*	22.94	0.12	ALFOSC
59732.22	*g*	23.18	0.06	LMI
59732.22	*r*	23.06	0.06	LMI
59732.22	*i*	22.88	0.06	LMI
59752.98	*g*	23.82	0.14	ALFOSC
59753.0	*r*	23.48	0.12	ALFOSC
59753.01	*i*	23.46	0.14	ALFOSC
59767.91	*r*	25.8	0.58	ALFOSC
59767.91	*g*	26.77	99.0	ALFOSC
59767.92	*i*	25.41	0.48	ALFOSC
59769.0	*i*	23.2	0.2	LMI
59778.9	*r*	25.05	0.26	ALFOSC
59780.93	*i*	24.44	0.26	ALFOSC
59674.0	*u*	22.14	0.02	LBC
59674.0	*g*	22.15	0.02	LBC
59674.0	*r*	22.08	0.03	LBC
59674.0	*i*	22.1	0.04	LBC
59674.0	*z*	22.2	0.07	LBC
59690.0	*u*	22.59	0.07	LBC
59690.0	*g*	22.36	0.06	LBC
59690.0	*r*	22.36	0.06	LBC
59690.0	*i*	22.35	0.08	LBC
59690.0	*z*	22.51	0.15	LBC
59729.0	*u*	23.36	0.05	LBC
59729.0	*g*	23.16	0.04	LBC
59729.0	*r*	22.94	0.04	LBC
59729.0	*i*	22.94	0.08	LBC
59729.0	*z*	22.82	0.16	LBC
59768.0	*u*	24.71	0.35	LBC
59768.0	*g*	24.2	0.19	LBC
59768.0	*r*	23.79	0.15	LBC
59768.0	*i*	23.61	0.16	LBC
59768.0	*z*	23.21	0.21	LBC
59732.2	*g*	23.18	0.06	LMI
59732.21	*r*	23.06	0.06	LMI
59732.22	*i*	22.88	0.06	LMI
59769.23	*i*	23.19	0.14	LMI

Note. New observations of AT 2022cmc since its discovery in I. Andreoni et al. (2022).

(This table is available in machine-readable form in the online article.)

slight differences from the ZTF photometric system. This is accounted for when fitting the light curve and SED.

ORCID iDs

Erica Hammerstein https://orcid.org/0000-0002-5698-8703
S. Bradley Cenko https://orcid.org/0000-0003-1673-970X
Igor Andreoni https://orcid.org/0000-0002-8977-1498
Panos Charalampopoulos https://orcid.org/0000-0002-0326-6715
Ryan Chornock https://orcid.org/0000-0002-7706-5668
Raffaella Margutti https://orcid.org/0000-0003-4768-7586
Brendan O'Connor https://orcid.org/0000-0002-9700-0036
Steve Schulze https://orcid.org/0000-0001-6797-1889
Jesper Sollerman https://orcid.org/0000-0003-1546-6615
Sudhanshu Barway https://orcid.org/0000-0002-3927-5402
Varun Bhalerao https://orcid.org/0000-0002-6112-7609
G. C. Anupama https://orcid.org/0000-0003-3533-7183
Harsh Kumar https://orcid.org/0000-0003-0871-4641
Ester Marini https://orcid.org/0000-0002-6894-1267
Diego Paris https://orcid.org/0000-0002-7409-8114
Daniel A. Perley https://orcid.org/0000-0001-8472-1996
Andrea Rossi https://orcid.org/0000-0002-8860-6538
Yuhan Yao https://orcid.org/0000-0001-6747-8509

References

Andreoni, I., Coughlin, M. W., Perley, D. A., et al. 2022, Natur, 612, 430
Barthelmy, S. D., Barbier, L. M., Cummings, J. R., et al. 2005, SSRv, 120, 143
Bellm, E. C., Kulkarni, S. R., Graham, M. J., et al. 2019, PASP, 131, 018002
Berger, E., Zauderer, A., Pooley, G. G., et al. 2012, ApJ, 748, 36
Bertin, E. 2011, ASPC, 442, 435
Bertin, E., & Arnouts, S. 1996, A&AS, 117, 393
Bertin, E., Mellier, Y., Radovich, M., et al. 2002, ASPC, 281, 228
Bloom, J. S., Giannios, D., Metzger, B. D., et al. 2011, Sci, 333, 203
Brown, G. C., Levan, A. J., Stanway, E. R., et al. 2015, MNRAS, 452, 4297
Brown, G. C., Levan, A. J., Stanway, E. R., et al. 2017, MNRAS, 472, 4469
Burrows, D. N., Kennea, J. A., Ghisellini, G., et al. 2011, Natur, 476, 421
Cendes, Y., Berger, E., Alexander, K. D., et al. 2024, ApJ, 971, 185
Cenko, S. B., Krimm, H. A., Horesh, A., et al. 2012, ApJ, 753, 77
Chambers, K. C., Magnier, E. A., Metcalfe, N., et al. 2016, arXiv:1612.05560
Charalampopoulos, P., Leloudas, G., Malesani, D. B., et al. 2022, A&A, 659, A34
Dai, L., McKinney, J. C., Roth, N., Ramirez-Ruiz, E., & Miller, M. C. 2018, ApJL, 859, L20
De Colle, F., & Lu, W. 2020, NewAR, 89, 101538
Eftekhari, T., Tchekhovskoy, A., Alexander, K. D., et al. 2024, ApJ, 974, 149
Fontana, A., Dunlop, J. S., Paris, D., et al. 2014, A&A, 570, A11
Foreman-Mackey, D., Hogg, D. W., Lang, D., & Goodman, J. 2013, PASP, 125, 306
Frank, J., & Rees, M. J. 1976, MNRAS, 176, 633
Gehrels, N., Chincarini, G., Giommi, P., et al. 2004, ApJ, 611, 1005
Gelman, A., Roberts, G. O., & Gilks, W. R. 1996, in Bayesian Statistics, ed. J. M. Bernardo et al. (Oxford Univ. Press), 599
Gezari, S. 2021, ARA&A, 59, 21
Gezari, S., Chornock, R., Rest, A., et al. 2012, Natur, 485, 217
Graham, M. J., Kulkarni, S. R., Bellm, E. C., et al. 2019, PASP, 131, 078001
Guillochon, J., Manukian, H., & Ramirez-Ruiz, E. 2014, ApJ, 783, 23
Guolo, M., Gezari, S., Yao, Y., et al. 2024, ApJ, 966, 160
Hammerstein, E., Cenko, S. B., Gezari, S., et al. 2023b, ApJ, 957, 86
Hammerstein, E., Gezari, S., van Velzen, S., et al. 2021, ApJL, 908, L20
Hammerstein, E., van Velzen, S., Gezari, S., et al. 2023a, ApJ, 942, 9
Hill, J. M., Green, R. F., Slagle, J. H., et al. 2008, Proc. SPIE, 7012, 701203
Hills, J. G. 1975, Natur, 254, 295
Hinkle, J. T., Holoien, T. W. S., Shappee, B. J., et al. 2020, ApJL, 894, L10
Hinshaw, G., Larson, D., Komatsu, E., et al. 2013, ApJS, 208, 19
Jiang, Y.-F., Guillochon, J., & Loeb, A. 2016, ApJ, 830, 125
Jonker, P. G., Stone, N. C., Generozov, A., van Velzen, S., & Metzger, B. 2020, ApJ, 889, 166
Komossa, S., & Bade, N. 1999, A&A, 343, 775
Kumar, H., Bhalerao, V., Anupama, G. C., et al. 2022a, AJ, 164, 90
Kumar, H., Bhalerao, V., Anupama, G. C., et al. 2022b, MNRAS, 516, 4517
Law-Smith, J., Ramirez-Ruiz, E., Ellison, S. L., & Foley, R. J. 2017, ApJ, 850, 22
Levan, A. J., Tanvir, N. R., Cenko, S. B., et al. 2011, Sci, 333, 199
Levan, A. J., Tanvir, N. R., Brown, G. C., et al. 2016, ApJ, 819, 51
Loeb, A., & Ulmer, A. 1997, ApJ, 489, 573
Lu, W., & Bonnerot, C. 2020, MNRAS, 492, 686
Masterson, M., De, K., Panagiotou, C., et al. 2024, ApJ, 961, 211
Mummery, A., van Velzen, S., Nathan, E., et al. 2024, MNRAS, 527, 2452
Nicholl, M., Lanning, D., Ramsden, P., et al. 2022, MNRAS, 515, 5604
Oke, J. B., Cohen, J. G., Carr, M., et al. 1995, PASP, 107, 375
Pasham, D., Gendreau, K., Arzoumanian, Z., & Cenko, B. 2022, GCN, 31601, 1
Pasham, D. R., Cenko, S. B., Levan, A. J., et al. 2015, ApJ, 805, 68
Pasham, D. R., Lucchini, M., Laskar, T., et al. 2023, NatAs, 7, 88
Perley, D. A. 2022, GCN, 31592, 1
Piran, T., Svirski, G., Krolik, J., Cheng, R. M., & Shiokawa, H. 2015, ApJ, 806, 164
Rhodes, L., Bright, J. S., Fender, R., et al. 2023, MNRAS, 521, 389
Sazonov, S., Gilfanov, M., Medvedev, P., et al. 2021, MNRAS, 508, 3820
Shappee, B. J., Prieto, J. L., Grupe, D., et al. 2014, ApJ, 788, 48
Silverman, J. M., Foley, R. J., Filippenko, A. V., et al. 2012, MNRAS, 425, 1789
Somalwar, J. J., Ravi, V., Dong, D. Z., et al. 2025, ApJ, 982, 163
Speziali, R., Di Paola, A., Giallongo, E., et al. 2008, Proc. SPIE, 7014, 70144T
Steele, I. A., Smith, R. J., Rees, P. C., et al. 2004, Proc. SPIE, 5489, 679
Tanvir, N. R., de Ugarte Postigo, A., Izzo, L., et al. 2022, GCN, 31602, 1
Tchekhovskoy, A., Metzger, B. D., Giannios, D., & Kelley, L. Z. 2014, MNRAS, 437, 2744
van Velzen, S., Gezari, S., Hammerstein, E., et al. 2021, ApJ, 908, 4
Yao, Y., Alexander, K. D., Lu, W., et al. 2025, ApJ, 993, 198
Yao, Y., Guolo, M., Tombesi, F., et al. 2024b, ApJ, 976, 34
Yao, Y., Lu, W., Harrison, F., et al. 2024a, ApJ, 965, 39
Yao, Y., Ravi, V., Gezari, S., et al. 2023, ApJL, 955, L6
Zauderer, B. A., Berger, E., Soderberg, A. M., et al. 2011, Natur, 476, 425